**MATERIALE PLASTICE**
*https://revmaterialeplastice.ro*
*https://doi.org/10.37358/Mat.Plast.1964*

# A Simplified Fabrication Approach for PMMA Resists in Electron-Beam Lithography

**BANGCHI HUANG[1,2], QIANYI YANG[1,2], XIANG LI[1,2], JIANLIN SHI[1,2], ZHIPENG ZHONG[1,2], YEZHAO ZHUANG[1,2], HAI HUANG[1,2*]**

[1] State Key Laboratory of Photovoltaic Science and Technology, Shanghai Frontiers Science Research Base of Intelligent Optoelectronic and Perception, Institute of Optoelectronics and College of Future Information Technology, Fudan University, Shanghai, 200433, China

[2] College of Smart Materials and Future Energy, Fudan University, Shanghai, 200433, China

***Abstract:*** *Lithography is a core-pattern transfer technique in micro/nanofabrication, among which electron-beam lithography (EBL) is a representative example. Polymethyl methacrylate (PMMA) has been widely employed as an electron-beam resist due to its high sensitivity, high resolution, and excellent contrast. However, commercial PMMA resists are relatively expensive and have complex formulations, thereby limiting process flexibility and cost control. Here, we demonstrate a rapid, low-cost preparation method for a PMMA resist suitable for micrometer-scale EBL. PMMA powder was dissolved in anisole to obtain a 4 wt% solution, which was spin-coated onto substrates to form uniform and smooth thin films. To evaluate resist performance, a custom-designed 5 × 5 array pattern was used to systematically study the effect of exposure dose on pattern quality. Results show that doses below 200 μC/cm² fail to induce complete scission of the PMMA molecular chains. Thermal evaporation and a lift-off process were employed to verify the dimensional accuracy of fabricated electrodes. Within the exposure dose range of 240–270 μC/cm², the electrode patterns were complete and exhibited straight edges. The optimal pattern fidelity was achieved at 260 μC/cm², with an absolute dimensional error below 0.2 μm, meeting the precision requirements of most micro/nanofabrication applications. This work provides a practical process reference for the preparation of PMMA electron-beam resists and their application in nanodevice fabrication.*

***Keywords:*** *Electron-beam lithography, polymethyl methacrylate, resist, exposure dose*

## 1. Introduction

Lithography is one of the most fundamental pattern transfer techniques in the field of micro/nanofabrication [1–3]. Lithography employs radiation sources (photons, electron beams, and ion beams) to selectively expose photosensitive or radiation-sensitive materials. After development, the desired micro- and nanostructures can be obtained. By methodology, lithography can be classified into ultraviolet (UV) lithography [4,5], electron-beam lithography (EBL) [6–8], X-ray lithography [9], scanning probe lithography (SPL) [10], and nanoimprint lithography (NIL) [11]. Among these, EBL, as a direct-write technique based on the point-by-point scanning of a focused electron beam and offers distinct advantages, including maskless processing, high patterning flexibility, and excellent resolution [2,12,13]. It has become an indispensable technique for high-precision patterning in areas such as nanoelectronics [14–16], photonics [17], and quantum devices [18].

In EBL, the ultimate patterning resolution is limited by the performance of the electron-beam resist. Polymethyl methacrylate (PMMA) has been the resist of choice for high-resolution patterning since its introduction into the field in the 1960s [19,20]. PMMA is non-toxic, easy to process, and available in multiple molecular-weight grades [21–24]. It exhibits excellent film uniformity, stable performance, and high optical transparency in the visible range, enabling sub-10 nm patterning resolution in EBL

**email: huangh@fudan.edu.cn*

CC BY

[25–28]. Moreover, PMMA adheres well to a variety of substrates and can also be combined with UV lithography [29,30]. By adjusting exposure dose, bake temperature, and development conditions, PMMA can function as either a positive- or negative-tone resist [30,31]. However, most PMMA electron-beam resists currently used are commercial products containing high-purity solvents (e.g., anisole, chlorobenzene, ethyl lactate), crosslinkers, and other additives [19]. Their preparation often requires stringent raw-material purification and precise compositional control; the resultant complex manufacturing increases overall fabrication cost.

In this work, we developed a simplified method to prepare a PMMA electron-beam resist. Anisole was used as the solvent to prepare a 4 wt% PMMA solution, where PMMA powder was rapidly dissolved through magnetic stirring and constant-temperature heating. The resulting resist was spin-coated onto $Si/SiO_2$ substrates to form uniform thin films. To evaluate the performance of the PMMA resist, we used a custom-designed 5 × 5 array and systematically investigated the effects of exposure dose on pattern quality and dimensional accuracy. At low exposure doses ($<200$ μC/cm$^2$), scission of the PMMA molecular chains was incomplete, leading to underdevelopment and loss of features. To quantify dimensional fidelity, metal deposition followed by lift-off was used to measure the actual electrode dimensions produced over the 240–270 μC/cm$^2$ dose range. The best performance was obtained at 260 μC/cm$^2$, yielding an absolute error $<0.2$ μm for a 10-μm feature, confirming the suitability of the prepared PMMA resist for micrometer-scale fabrication. This study provides a cost-effective and high-performance process route for electron-beam lithography.

## 2. Materials and methods

Silicon substrates with a 285 nm $SiO_2$ layer were cut into pieces with dimensions of 6 cm × 3 cm using a laser scribing machine. The substrates were sequentially cleaned in acetone, isopropanol, and deionized water and ultrasonically agitated for 30 min in each solvent, then dried under nitrogen. To enhance resist-substrate adhesion, the samples were treated in an ozone (plasma) cleaner for 10 min. During spin coating, the resist was first spread at a low speed of 600 rpm for 10 s, followed by a high-speed spin at 4000 rpm for 40 s to form a uniform film. After spin coating, the samples were baked on a hot plate at 180°C for 3 min to remove residual solvent (pre-bake). The exposure array pattern was designed using KLayout software. Electron-beam lithography was performed using a VEGA LMS system (TESCAN, Czech Republic) at an accelerating voltage of 30 keV and a beam current of 300 pA. The developer consisted of 4-methyl-2-pentanone and isopropanol (IPA) mixed in a volume ratio of 1:3. The samples were developed for 8 s and then rinsed in IPA to remove residual developer from the surface. Metal deposition was carried out by thermal evaporation to deposit a 120 nm-thick Ag film. Prior to deposition, the chamber was evacuated for 2 h until the base pressure reached $3.0 \times 10^{-4}$ Pa. After deposition, the samples were immersed in acetone to lift off the unwanted metal and resist, followed by rinsing with IPA to remove any residual acetone. Finally, the fabricated electrode patterns were examined and characterized using an optical microscope.

## 3. Results and discussions

Figure 1 illustrates the preparation process of the PMMA electron-beam resist. First, an appropriate amount of PMMA powder (molecular weight: $1 \times 10^5$, particle diameter: 100 μm) was weighed and placed into a clean beaker. Anisole was then added as the solvent, which effectively dissolve PMMA and promotes resist uniformity. The beaker was placed on a temperature-controlled hot plate with magnetic stirring at 50°C, and stirred continuously at 300–500 rpm to fully dissolve the PMMA powder, forming a transparent and homogeneous solution. Maintaining a constant temperature accelerates the dispersion and dissolution of the polymer chains in the solvent, while preventing excessive solvent evaporation. Once the PMMA powder was completely dissolved, the beaker was removed from the hot plate and

allowed to cool to room temperature to minimize any thermal mismatch effects on subsequent spin-coating film quality. The resulting PMMA resist solution exhibited moderate viscosity and good fluidity, making it suitable for direct use in the subsequent electron-beam lithography process.

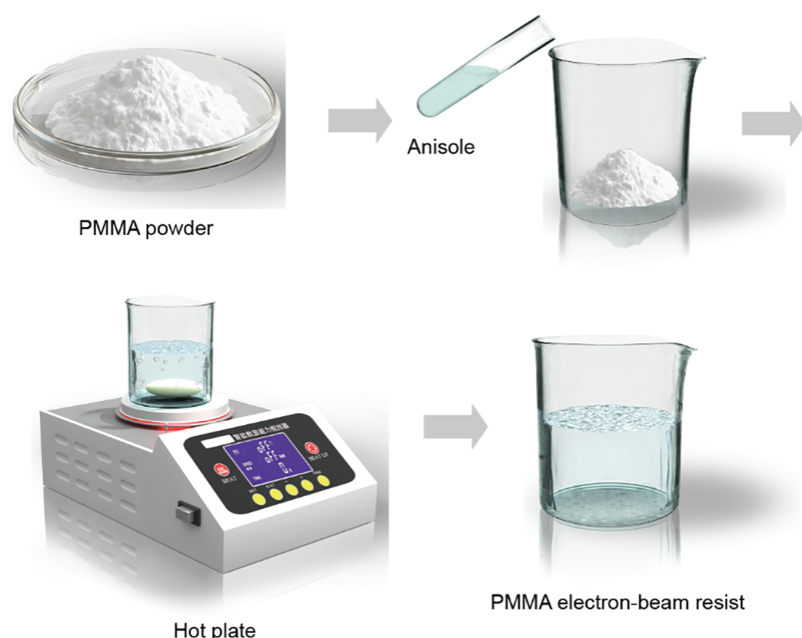


**Figure 1.** Schematic illustration of the preparation process for PMMA electron-beam resist. A measured mass of PMMA powder was added to a defined volume of anisole in a beaker. The mixture was heated at constant temperature on a hot plate with magnetic stirring until fully dissolved, the PMMA electron-beam resist was obtained

Figure 2 demonstrates the spin-coating process of PMMA onto a $Si/SiO_2$ substrate, employing a double-layer resist structure of MMA/PMMA. First, a silicon substrate with dimensions of 6 cm × 3 cm was selected and fixed onto the vacuum chuck of the spin coater. A suitable amount of MMA resist was dispensed onto the substrate surface using a pipette. Following the preset spin-coating parameters (see Materials and Methods), the MMA layer was evenly spread over the substrate. After spin coating, the sample was baked on a hot plate and then cooled to room temperature. Subsequently, PMMA resist was dispensed onto the MMA-coated substrate, and the same spin-coating and baking procedures were repeated. It is worth noting that the PMMA thickness is governed by spin speed and coating time. Under the selected parameters in this work, a uniform, dense, and smooth PMMA film was obtained on the substrate surface, meeting the uniformity requirements for subsequent electron-beam lithography.

To evaluate the performance parameters of the prepared PMMA resist during the electron-beam lithography process, an electrode array pattern was designed (Figure 3a). The layout is a periodic 5 × 5 array (700 μm × 700 μm; 0.49 $mm^2$), enabling the fabrication of electrode units under different parameter conditions within a single exposure. This design effectively minimizes batch-to-batch process variations, thereby providing a reliable basis for subsequent optimization of the exposure dose. Figure 3b presents an enlarged schematic of a single unit, which contains multiple electrode structures with different widths (10 μm, 5 μm, 2 μm, and 1 μm) and spacings (7.5 μm, 6.5 μm, 2 μm, and 1 μm). By comparing the fabricated patterns of electrodes with various dimensions after exposure and development, the optimal exposure dose range can be determined.

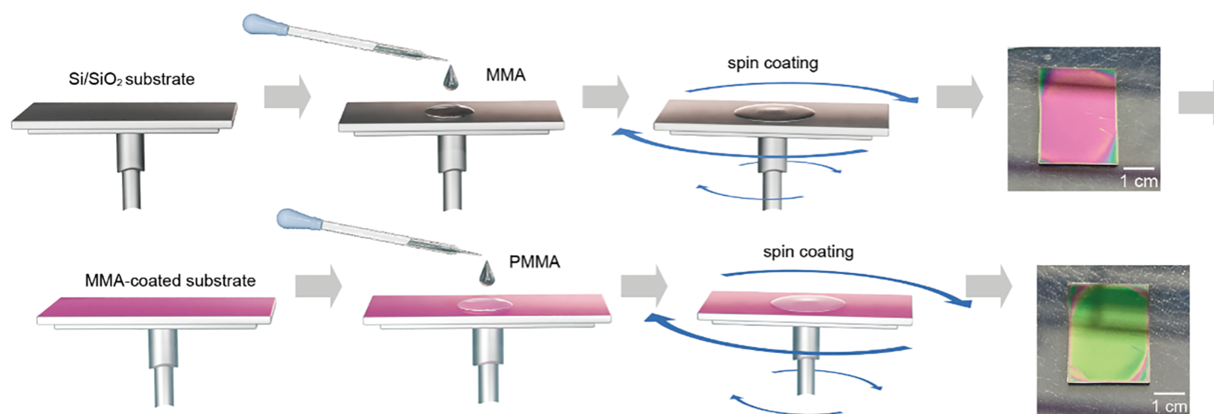


**Figure 2.** Process flow for spin-coating PMMA electron-beam resist on a $Si/SiO_2$ substrate

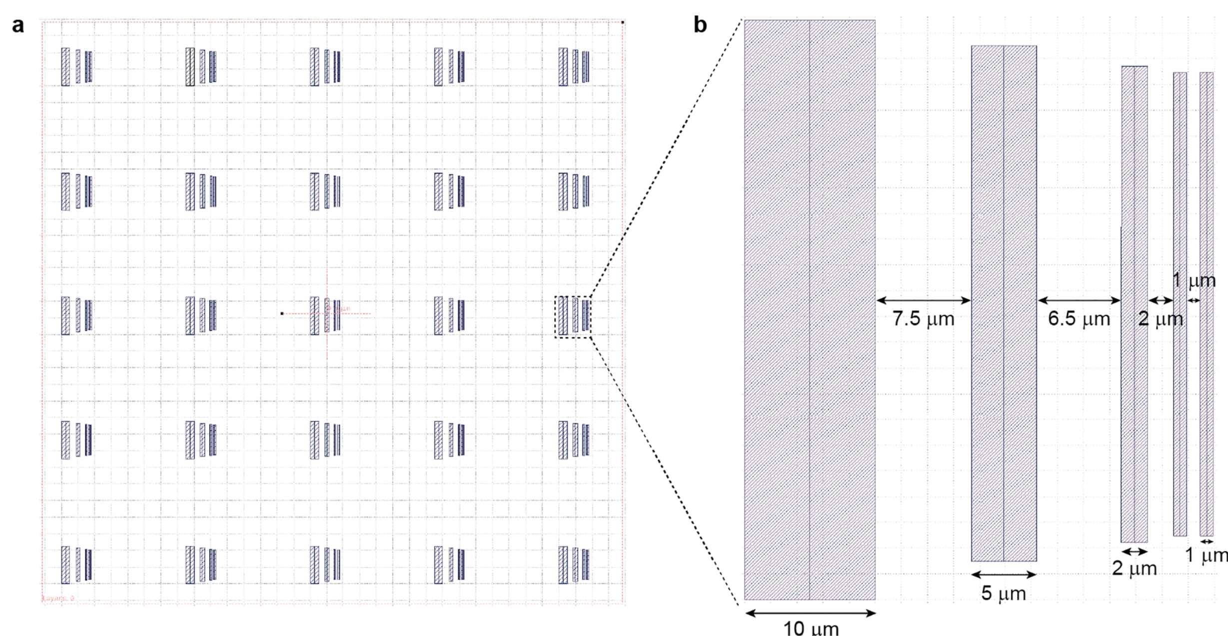


**Figure 3.** Design layout and structural dimensions of the electrode array for electron-beam lithography. (**a**) Overall layout of periodically arranged multi-electrode units, covering a total area of 700 µm × 700 µm. (**b**) Enlarged view of a single unit, indicating the widths of the electrodes (10 µm, 5 µm, 2 µm, and 1 µm) and the corresponding gaps (7.5 µm, 6.5 µm, 2 µm, and 1 µm)

During exposure, the interaction mechanism between the PMMA resist and the electron beam is a key factor influencing the fidelity of the patterned structures. The prepared PMMA functions as a positive-tone resist, undergoing scission of its C-C backbone under electron-beam irradiation, thereby generating low-molecular-weight fragments that are selectively dissolved during development [32] (Figure 4a). Figure 4b presents optical micrographs of the developed patterns obtained under exposure doses ranging from 100 to 350 µC/cm$^2$. The results show that at doses below 150 µC/cm$^2$, the pattern edges appear indistinct, owing to insufficient scission of the C-C backbone, some fine features are nearly absent after development [33]. In contrast, at doses above 280 µC/cm$^2$, narrow-gap regions exhibit feature merging, and the resolution of 1 µm and 2 µm gaps is significantly reduced. This is attributed to excessive exposure, where scattered electrons also cause development of areas adjacent to the intended

cc BY

exposure region, leading to a pronounced proximity effect [34,35]. Within 240–270 μC/cm$^2$, the pattern edges remain straight and sharp, and the fine-line structures exhibit high fidelity, indicating excellent pattern transfer performance.

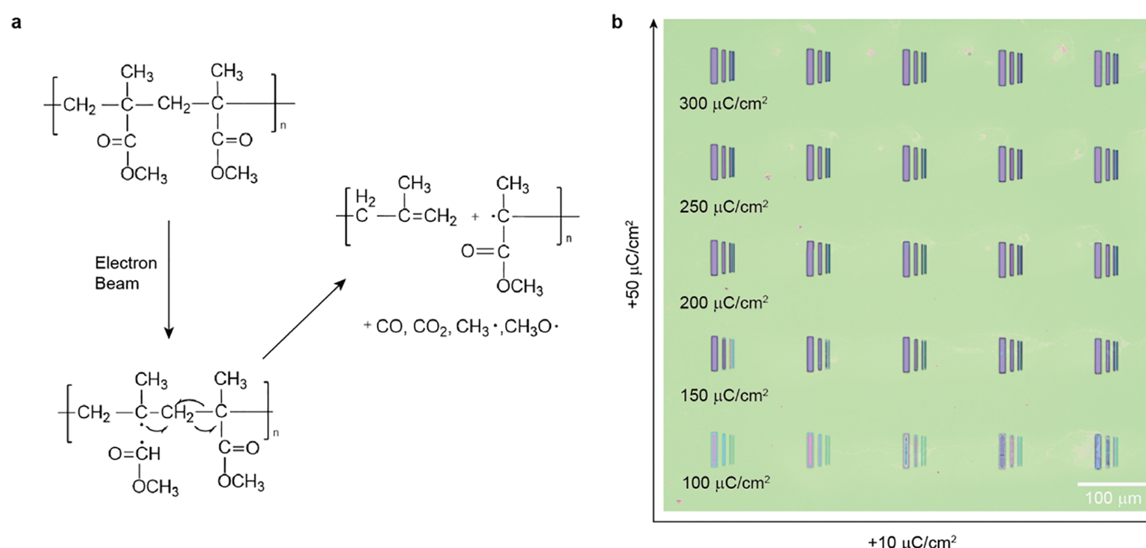


**Figure 4.** Principle of beam exposure and patterning results under different exposure doses. (**a**) Schematic illustration of the molecular chain scission reaction in PMMA induced by electron-beam irradiation, showing the main-chain cleavage and generation of low-molecular-weight fragments caused by high-energy electron bombardment. (**b**) Optical micrographs of electrode array patterns obtained at different exposure doses (100–350 μC/cm$^2$). The horizontal and vertical axes represent the directions of increasing exposure dose, scale bar: 100 μm

To evaluate the practical applicability of the PMMA resist, a metal deposition and lift-off process was performed following development (Figure 5a). Specifically, a 120 nm-thick Ag film was deposited onto the developed sample in a high-vacuum environment, ensuring uniform coverage across the entire substrate surface. The sample was then immersed in an acetone solution to remove the resist along with the overlying metal, thereby retaining only the metal patterns deposited directly on the exposed substrate regions. Figure 5b presents the resulting metal electrode arrays fabricated under different exposure doses. When the exposure dose was in the range of 100–140 μC/cm$^2$, the dose was insufficient for complete development, resulting in the absence of electrode patterns on the substrate. Although coarse electrodes could be observed after development at doses of 150–190 μC/cm$^2$, almost no metal patterns remained after lift-off, indicating that exposure doses below 200 μC/cm$^2$ are insufficient for accurate metal pattern transfer. Figure 5c compares four representative exposure conditions—240, 250, 260, and 270 μC/cm$^2$—that yielded higher-resolution features. While all four conditions produced patterns of generally high quality, slight variations were observed: at 240 μC/cm$^2$, the narrowest lines exhibited minor width reduction, whereas at 270 μC/cm$^2$, the resolution of the smallest gaps was slightly degraded. Nevertheless, these deviations did not significantly affect the overall pattern fidelity, and the electrode arrays retained well-defined and continuous features.

To quantitatively evaluate the impact of exposure dose on dimensional accuracy, we measured the dimensions of electrode patterns after metal deposition and calculated their absolute errors, focusing on the 240–270 μC/cm$^2$ dose window that exhibited superior morphology in optical micrographs. For each designed linewidth, ten repeated measurements were taken at different locations; the mean was taken as the measured dimension for that dose. Figure 6a summarizes the results; error bars denote the standard error of the mean. Across the four designed linewidths (1, 2, 5, and 10 μm), features

**MATERIALE PLASTICE**
*https://revmaterialeplastice.ro*
*https://doi.org/10.37358/Mat.Plast.1964*

written within this dose range displayed straight edges and small dimensional fluctuations. In evaluating lithographic precision, the absolute error—defined as the difference between the measured and designed dimensions—is a key metric. Using the smallest linewidth of 1 μm as an example (Figure 6b), increasing the dose from 240 to 260 μC/cm$^2$ reduced the absolute error from 0.064 to 0.015 μm, indicating a marked improvement in pattern fidelity. However, further increasing the dose to 270 μC/cm$^2$ raised the absolute error to 0.082 μm, primarily because sub-micrometer features are susceptible to proximity-effect overexposure at higher doses. These results identify 260 μC/cm$^2$ as the optimal dose under the present process conditions. At this optimal dose (260 μC/cm$^2$), the absolute error as a function of linewidth is shown in Figure 6c. Although the error increases with the designed dimension, the deviation at 10 μm is only 0.18 μm. Overall, the PMMA resist enables high-precision pattern transfer across the micrometer regime and meets the dimensional-accuracy requirements of most nanodevice fabrication processes.

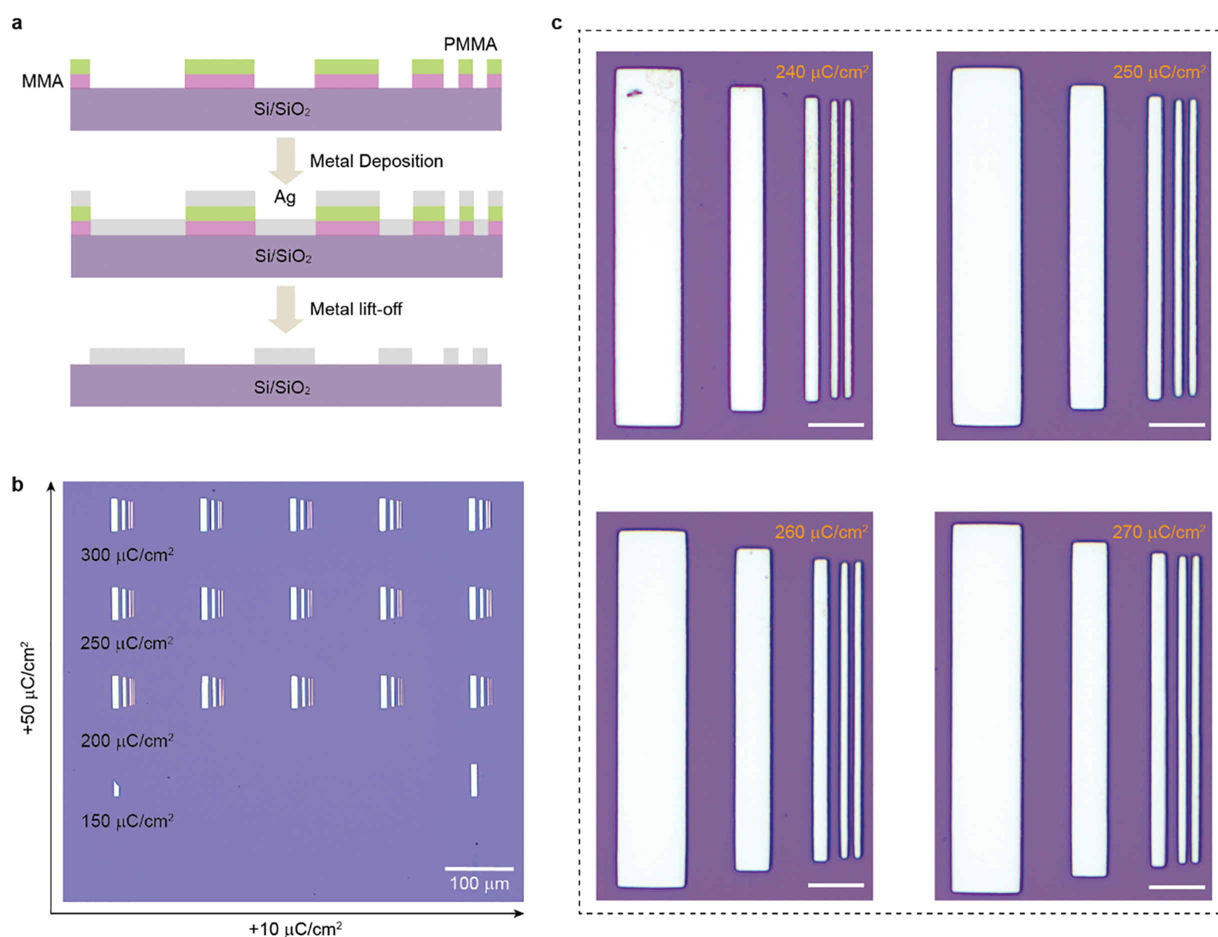


**Figure 5.** Metal deposition and lift-off process, and electrode patterns obtained under different exposure doses. (**a**) Schematic illustration of the metal deposition and lift-off process based on PMMA resist, including metal deposition and the subsequent lift-off to obtain electrode patterns. (**b**) Optical micrographs of electrode arrays fabricated under different exposure doses (150–300 μC/cm$^2$), with the horizontal and vertical axes representing the incremental directions of exposure dose, scale bar: 100 μm. (**c**) Enlarged optical micrographs of individual electrode units obtained at exposure doses of 240, 250, 260, and 270 μC/cm$^2$, showing the effect of dose variation on line clarity and pattern integrity, scale bar: 10 μm

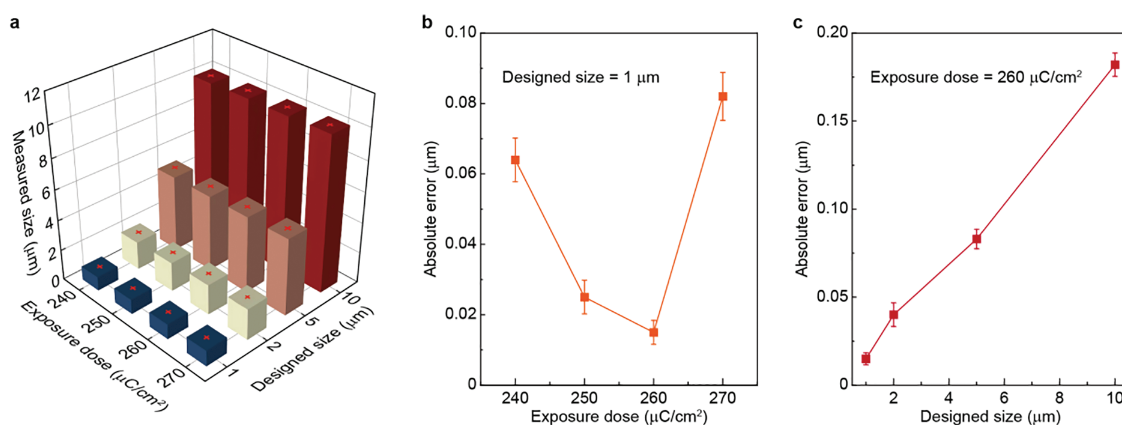


**Figure 6.** Error analysis of electrode dimensions under different exposure doses. (**a**) Comparison between designed and measured electrode dimensions at exposure doses of 240, 250, 260, and 270 $\mu C/cm^2$. (**b**) Absolute error for electrodes with a designed linewidth of 1 µm as a function of exposure dose. (c) Absolute error for electrodes with designed linewidths of 1, 2, 5, and 10 µm at an exposure dose of 260 $\mu C/cm^2$. The error bar represents the standard deviation of the statistical results

## 4. Conclusions

In this work, anisole was employed as the solvent to achieve the rapid preparation of a 4 wt% PMMA electron-beam resist. Uniform, smooth, and dense PMMA films were obtained on $Si/SiO_2$ substrates via spin coating. A systematically designed 5 × 5 electrode array pattern was used to evaluate the performance of the PMMA resist. The results showed that at exposure dose below 200 $\mu C/cm^2$, the dose was insufficient to induce adequate main-chain scission of PMMA, leading to incomplete development. A 120-nm-thick Ag film was subsequently deposited by thermal evaporation and patterned by lift-off. For features written at doses of 240–270 $\mu C/cm^2$, the patterned electrodes were complete with sharp edges; the best dimensional precision was obtained at 260 $\mu C/cm^2$, where the absolute error for a 10-µm feature was <0.2 µm. This precision meets the requirements of most micro/nanofabrication processes and provides a reliable process foundation for the fabrication of nano-optoelectronic devices. This cost-effective approach is readily applicable to academic and industrial EBL workflows. Finally, given the limited stability of the PMMA solution, this approach is advantageous for direct and timely use in lithography.

**Acknowledgement:** The authors acknowledge the Fudan Nanofabrication Laboratory for providing access to advanced equipment and technical support.

**Funding Statement:** This work was supported by the National Natural Science Foundation of China (Grants No. 12204109).

**Author Contributions:** The authors confirm contribution to the paper as follows: Conceptualization, Data curation, Formal analysis, Writing—original draft, Writing—review & editing: Bangchi Huang; Methodology, Investigation: Qianyi Yang; Conceptualization, Data curationg: Xiang Li; Formal analysis: Jianlin Shi; Investigation: Zhipeng Zhong; Methodology: Yezhao Zhuang; Data curation, Funding acquisition, Writing—original draft: Hai Huang. All authors reviewed the results and approved the final version of the manuscript.

**Availability of Data and Materials:** The data that support the findings of this study are available from the corresponding author upon reasonable request.

**Ethics Approval:** This study does not involve human or animal subjects.

**Conflicts of Interest:** The authors declare no conflicts of interest to report regarding the present study.

# References

1. Fischer J, Wegener M. Three-dimensional optical laser lithography beyond the diffraction limit. Laser Photonics Rev. 2013;7(1):22–44. doi:10.1002/lpor.201100046.
2. Qiao Y, Li C, Yan F, Liu Z, Wang X, Xie J, et al. Synergistic enhancement effects of heterogeneous isomorphism clusters in response to irradiation: sub-10 nm nanolithography and nanoscale etching transfer. Nano Lett. 2025;25(19):7732–9. doi:10.1021/acs.nanolett.5c00583.
3. Yang Y, Liu K, Gao Y, Wang C, Cao L. Advancements and challenges in inverse lithography technology: a review of artificial intelligence-based approaches. Light Sci Appl. 2025;14(1):250. doi:10.1038/s41377-025-01923-w.
4. Wu L, Hilbers MF, Lugier O, Thakur N, Vockenhuber M, Ekinci Y, et al. Fluorescent labeling to investigate nanopatterning processes in extreme ultraviolet lithography. ACS Appl Mater Interfaces. 2021;13(43):51790–8. doi:10.1021/acsami.1c16257.
5. Wang X, Tao P, Wang Q, Zhao R, Liu T, Hu Y, et al. Trends in photoresist materials for extreme ultraviolet lithography: a review. Mater Today. 2023;67:299–319. doi:10.1016/j.mattod.2023.05.027.
6. Luo T, Pan B, Zhang K, Dong Y, Zou C, Gu Z, et al. Electron beam lithography induced doping in multilayer $MoTe_2$. Appl Surf Sci. 2021;540:148276. doi:10.1016/j.apsusc.2020.148276.
7. Shahali H, Hasan J, Wang H, Tesfamichael T, Yan C, Yarlagadda PKDV. Evaluation of particle beam lithography for fabrication of metallic nano-structures. Procedia Manuf. 2019;30:261–7. doi:10.1016/j.promfg.2019.02.038.
8. Horák M, Bukvišová K, Švarc V, Jaskowiec J, Křápek V, Šikola T. Comparative study of plasmonic antennas fabricated by electron beam and focused ion beam lithography. Sci Rep. 2018;8(1):9640. doi:10.1038/s41598-018-28037-1.
9. Nazmov V, Goldenberg B, Vasiliev A, Asadchikov V. Optimization of X-ray lithography conditions for fabrication of large arrays of high-aspect-ratio submicron pores. J Micromech Microeng. 2021;31(5):055011. doi:10.1088/1361-6439/abf331.
10. Howell ST, Grushina A, Holzner F, Brugger J. Thermal scanning probe lithography-a review. Microsyst Nanoeng. 2020;6:21. doi:10.1038/s41378-019-0124-8.
11. Unno N, Mäkelä T. Thermal nanoimprint lithography—a review of the process, mold fabrication, and material. Nanomaterials. 2023;13(14):2031. doi:10.3390/nano13142031.
12. Wang Q, Chen YF, Long SB, Niu JB, Wang CS, Jia R, et al. Fabrication and characterization of single electron transistor on SOI. Microelectron Eng. 2007;84(5–8):1647–51. doi:10.1016/j.mee.2007.01.261.
13. Zhao R, Wang X, Xu H, Wei Y, He X. Machine learning in electron beam lithography to boost photoresist formulation design for high-resolution patterning. Nanoscale. 2024;16(8):4212–8. doi:10.1039/d3nr04819e.
14. Wang X, Dai X, Wang H, Wang J, Chen Q, Chen F, et al. All-water etching-free electron beam lithography for on-chip nanomaterials. ACS Nano. 2023;17(5):4933–41. doi:10.1021/acsnano.2c12387.
15. Giza M, Mukhopadhyay K, Ravichandran H, Pannone A, Ghosh S, Das S. Exploring the application of gold-assisted exfoliation in large-scale integration of n-type and p-type 2D-FETs. Small Methods. 2025;9:2500559. doi:10.1002/smtd.202500559.
16. Zhang Q, Li E, Wang Y, Gao C, Wang C, Li L, et al. Ultralow-power vertical transistors for multilevel decoding modes. Adv Mater. 2023;35(3):e2208600. doi:10.1002/adma.202208600.
17. Li S, Liu X, Yang H, Zhu H, Fang X. Two-dimensional perovskite oxide as a photoactive high-$\kappa$ gate dielectric. Nat Electron. 2024;7(3):216–24. doi:10.1038/s41928-024-01129-9.
18. Zhong HS, Wang H, Deng YH, Chen MC, Peng LC, Luo YH, et al. Quantum computational advantage using photons. Science. 2020;370(6523):1460–3. doi:10.1126/science.abe8770.

19. Chen Y. Nanofabrication by electron beam lithography and its applications: a review. Microelectron Eng. 2015;135:57–72. doi:10.1016/j.mee.2015.02.042.
20. Gangnaik AS, Georgiev YM, Holmes JD. New generation electron beam resists: a review. Chem Mater. 2017;29(5):1898–917. doi:10.1021/acs.chemmater.6b03483.
21. Peng B, Van der Wee E, Imhof A, Van Blaaderen A. Synthesis of monodisperse, highly cross-linked, fluorescent PMMA particles by dispersion polymerization. Langmuir. 2012;28(17):6776–85. doi:10.1021/la301288r.
22. Dobisz EA, Brandow SL, Bass R, Shirey LM. Resolution of polymethyl methacrylate: molecular weights of 950 000 vs 50 000. Appl Phys Lett. 1999;74(26):4064–6. doi:10.1063/1.123262.
23. Peng B, Van Blaaderen A, Imhof A. Direct observation of the formation of liquid protrusions on polymer colloids and their coalescence. ACS Appl Mater Interfaces. 2013;5(10):4277–84. doi:10.1021/am400490h.
24. Peng B, Soligno G, Kamp M, de Nijs B, de Graaf J, Dijkstra M, et al. Site-specific growth of polymers on silica rods. Soft Matter. 2014;10(48):9644–50. doi:10.1039/c4sm01989j.
25. Nam K, Woo K, Ryul K, Lee H. High-resolution electron beam lithography of PMMA derivatives with Langmuir-Blodgett films. Synth Met. 1997;85(1–3):1407–8. doi:10.1016/S0379-6779(97)80295-0.
26. Vieu C, Carcenac F, Pépin A, Chen Y, Mejias M, Lebib A, et al. Electron beam lithography: resolution limits and applications. Appl Surf Sci. 2000;164(1–4):111–7. doi:10.1016/S0169-4332(00)00352-4.
27. Song W, Kong L, Tao Q, Liu Q, Yang X, Li J, et al. High-resolution van der Waals stencil lithography for 2D transistors. Small. 2021;17(29):2101209. doi:10.1002/smll.202101209.
28. Dong X, Shao YA, Ping H, Tong X, Wu Y, Zhang Y, et al. Effect of metal oxide deposition on the sensitivity and resolution of E-beam photoresist. ACS Appl Mater Interfaces. 2024;16(41):56019–30. doi:10.1021/acsami.4c08591.
29. Rahman F, Carbaugh DJ, Wright JT, Rajan P, Pandya SG, Kaya S. A review of polymethyl methacrylate (PMMA) as a versatile lithographic resist–With emphasis on UV exposure. Microelectron Eng. 2020;224:111238. doi:10.1016/j.mee.2020.111238.
30. Carbaugh DJ, Pandya SG, Wright JT, Kaya S, Rahman F. Combination photo and electron beam lithography with polymethyl methacrylate (PMMA) resist. Nanotechnology. 2017;28(45):455301. doi:10.1088/1361-6528/aa8bd5.
31. Schnauber P, Schmidt R, Kaganskiy A, Heuser T, Gschrey M, Rodt S, et al. Using low-contrast negative-tone PMMA at cryogenic temperatures for 3D electron beam lithography. Nanotechnology. 2016;27(19):195301. doi:10.1088/0957-4484/27/19/195301.
32. Ali U, Karim KJBA, Buang NA. A review of the properties and applications of poly (methyl methacrylate) (PMMA). Polym Rev. 2015;55(4):678–705. doi:10.1080/15583724.2015.1031377.
33. Muchová M, Pelzbauer Z. The lithographic effect of electron beam on poly(methyl methacrylate) in a scanning electron microscope: minimization of line width by the dose and beam current. J Appl Polym Sci. 1989;37(3):817–24. doi:10.1002/app.1989.070370317.
34. Kostic I, Vutova K, Koleva E, Bencurova A. PMMA resist profile and proximity effect dependence on the electron-beam lithography process parameters. J Phys Conf Ser. 2020;1492(1):012015. doi:10.1088/1742-6596/1492/1/012015.
35. Nemec P, Vutova K, Bencurova A, Andok R, Kostic I. Comparative study of the sidewall shape and proximity effect in bilayer electron beam resist systems. J Phys Conf Ser. 2024;2710(1):012011. doi:10.1088/1742-6596/2710/1/012011.

Received: 15 August 2025; Accepted: 29 August 2025; Published: 30 September 2025